# An improved argument principle root-search method for modes of slab waveguides, optical fibers, and spheres

Sravya Rao[a,1,*], Parry Y. Chen[a,1], Yonatan Sivan[a]

[a]*School of Electrical and Computer Engineering, Ben-Gurion University, Israel*

## Abstract

We update our root-search method for transcendental equations. Our method is globally convergent and is guaranteed to locate all complex roots within a specified search domain, since it is based on Cauchy's residue theorem. We extend the implementation to treat the dispersion relations of slab waveguides and the resonances of a sphere, in addition to step-index fibers. We also implement other improvements, such as to the contour selection procedure to ensure the method remains reliable even in challenging parameter regimes.

*Keywords:* Complex root search; Argument principle method; Optical waveguide dispersion relation.

---

*Corresponding author - *E-mail address:* sravya@post.bgu.ac.il
[1]Equal contributors to this update

geometries and applicability in determining the radiative modes in the context of propagation constant modes.

*Summary of revisions:* To ensure the method is reliable even in challenging parameter regimes, we make several revisions in the contour selection strategy like enlargment of contour for lower-order roots, implementing elliptical shaped contours and employing adaptive scheme for higher-order roots. Additionally, we also rescale the search variables in the context of propagation constant when spacing between roots is large.

We also demonstrate the extension of the method to slab & sphere geometries, and computation of radiative modes.

*Nature of problem:* Locating the complex roots of a general transcendental equation is often a non-trivial task. Iterative methods such as Newton's method face numerous difficulties because the existence of roots with narrow and otherwise difficult attraction basins requires very accurate initial guesses to locate. Robust location of a complete set of roots thus becomes problematic. In optics, modes of a circular fiber are obtained from a transcendental equation, the dispersion relation. Several recent advancements in optics have necessitated its robust solution, including the fabrication of high index contrast fibers and analytical methods that expand radiating sources using eigenmodes.

*Solution method:* We employ the argument principle method, a robust globally convergent method guaranteed to locate all roots in the specified search domain. It is based on the Cauchy residue theorem, and projects the locations of the roots on to a polynomial basis. Unlike previous implementations of the argument principle method [2,3] and related methods [4], our implementation has two features vital for solving the fiber dispersion relation. It allows isolated singularities within the search domain, and allows the search domain to approach arbitrarily close to branch points without experiencing failure. Furthermore, our simple MATLAB implementation is designed to be easily modified and integrated for a variety of applications.

*Additional comments including restrictions and unusual features (approx. 50-250 words):* The specified search domain must be meromorphic, in other words be complex analytic containing at most isolated singularities. The locations and orders of these singularities must be known analytically, so we describe how they are determined for our fiber dispersion relation. Branch points and branch cuts must be avoided, though the search domain may be arbitrarily close. We exploit knowledge of our dispersion relation, specifically that roots are located close to singularities, to simplify the method.

## References

[1] P. Y. Chen, Y. Sivan, Robust location of optical fiber modes via the argument principle method, Comput. Phys. Commun. 214 (2017) 105–116.
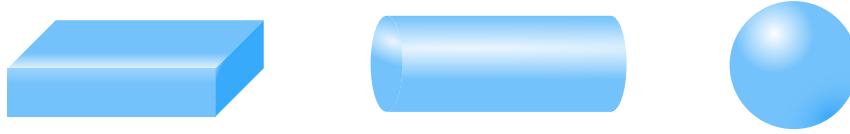
FIGURE 1: *The three geometries treated in this update: a slab waveguide with infinite translational symmetry in two dimensions, a circular fiber infinitely extended in one direction, and a sphere.*

[2] L. C. Botten, M. S. Craig, R. C. McPhedran, Complex zeros of analytic functions, Comput. Phys. Commun. 29 (3) (1983) 245–259.

[3] P. Kravanja, M. Van Barel, O. Ragos, M. N. Vrahatis, F. A. Zafiropoulos, ZEAL: A mathematical software package for computing zeros of analytic functions, Comput. Phys. Commun. 124 (2–3) (2000) 212–232.

[4] C. J. Gillan, A. Schuchinsky, I. Spence, Computing zeros of analytic functions in the complex plane without using derivatives, Comput. Phys. Commun. 175 (4) (2006) 304–313.

## 1. Introduction

In this update, we revisit our original algorithm,[1] where we implemented a robust, globally convergent argument principle root-search subroutine for transcendental equations. The algorithm is guaranteed to locate all roots within a specified search domain of the complex plane, since it is a globally convergent algorithm based on Cauchy's residue theorem. We applied the algorithm to treat the step-index optical fiber dispersion relation, i.e., to find dispersion curves ($\omega$-frequency vs $\beta$-propagation constant[2, 3], or $\beta$-modes in short) given a user-specified fiber radius and material dispersion relation. Free-to-use code was published alongside the original article.[1] The algorithm found the roots up to any desired order with minimal human supervision, and without any concerns of divergence with increased number of iterations.[4] The implementation can also search for permittivity as the eigenvalue, which is useful for defining the normal modes of open, unbounded systems.[5–27]

The first purpose of this update is to enhance the reliability of our implementation in the context of optical waveguide dispersion relations. Even though our original algorithm is mathematically guaranteed to locate all roots within a specified search domain, our original implementation is still liable to miss some of the roots. There are two possible reasons for this.

Firstly, if the search domain is not specified to be large enough to encompass all the roots, then roots that stray deep into the complex plane will be missed. This can occur under certain parameter regimes. Secondly, the algorithm might fail due to the limitations of finite precision arithmetic when the search variable becomes very small or very large. In this update, we revise the algorithm to resolve these issues, yielding a more reliable implementation.

The second purpose of this update is to extend the implementation of our algorithm to treat the dispersion relations of slab waveguide and spherical scatterers, see Figure 1. These dispersion relations are simpler than that of the step-index optical fiber, leading to simpler attraction basins. Thus, these root-searches are perhaps less challenging, and may be more amenable to simpler techniques than the one presented here, such as the locally convergent Newton's method. But given that the roots can lie in the complex plane, locally convergent techniques can still be unreliable, as their success is excessively dependent on good initial guesses. To ensure that roots are not missed, it is still beneficial to use our globally convergent algorithm.

The third purpose of this update is to demonstrate its applicability to compute the *radiative and leaky* optical waveguide ($\beta$) modes, i.e., those for which the search variable is a complex propagation constant $\beta$; previously, we studied such modes only when the search variable was the (eigen-) permittivity. Such mode are encountered also in the context of the Schrödinger equation in the description of electron states whose energies are above the vacuum level [28]; the optical formulation adopted below reduces to this case for a fixed value of the frequency.

This document is organized as follows. In Section 2, we motivate the need for enhancements to the algorithm, and then proceed to develop the necessary revisions and their implementations. In Section 3.1, we describe the implementation of the method to treat the (asymmetric) slab waveguide dispersion relation. This section incorporates the revisions of Section 2 and its implementation for the radiative and leaky modes. Section 3.2 provides a brief discussion of the implementation for spherical scatterers.

## 2. Revision of the Algorithm

In the original iteration of these utilities [1], the contour selection strategy was guided by two key observations: (a) there exists one root for each singularity, counting multiplicities, and (b) these roots are often located in the vicinity of their respective singularities. We thus devised a simple strategy to enclose all the roots with a set of overlapping contours, with one contour

centered on each singularity. This was specified in Eq. (13) of our original manuscript and demonstrated there in Figure 2. However, this strategy was liable to fail for some parameter regimes. This is because although observation (b) holds firm for the high-order roots, it is more tenuous for the first few roots, as these tend to stray the furthest from their respective singularities.
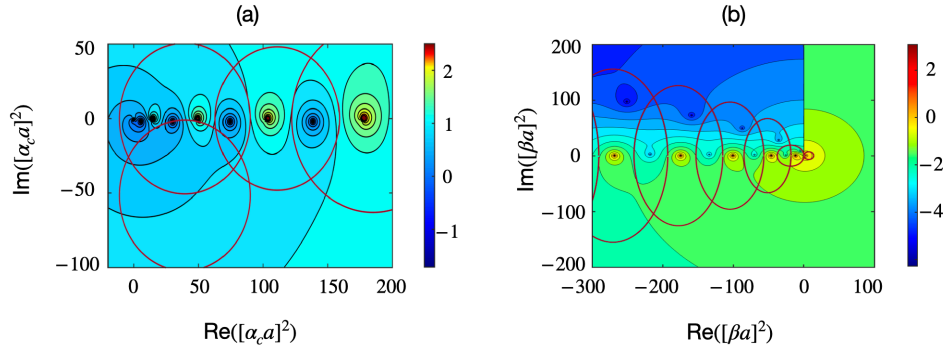


FIGURE 2: *Examples of the attraction basins and our revised contour selection strategy (magenta). Horizontal and vertical axes represent real and imaginary parts of the complex search variable domain, while color is the logarithmic magnitude of the transcendental equation, $\log_{10}(|f(z)|)$ (see equivalent figure in [1] for more details). Thus, the roots are deep blue and the singularities are red. Plot (a) shows the attraction basin of $(\alpha_c a)^2$ search variable with enlarged first contour (top leftmost) which now enclose the first couple of singularities, as well as the first 6 roots. It is described in Eq. (1). Another contour (Eq. (2)) is located below this contour to capture any plasmonic roots that wander further into the lower half of the complex plane. Plot (b) shows an example of an attraction basin of $(\beta a)^2$ search variable for which elliptical contour selection for higher order roots is more suitable.*

In this update, we revise our strategy for finding the first few roots, via a simple modification that has been tested to succeed even for challenging parameter regimes. In particular, we combine the first two contours into one large contour that covers a much larger region of the search space. Even so, this enlarged contour still does not enclose more than 6 roots, and thus not present any difficulties for the numerically sensitive Newton's identities. This contour is displayed in Figure 2. Specifically, we define the center and radius of this enlarged contour to be

$$
\begin{aligned}
c_1 &= \frac{3}{8}u_3 + \frac{1}{8}u_2 + \frac{1}{8}u_1 + \frac{3}{8}u_0, \\
r_1 &= \frac{3}{8}u_3 + \frac{1}{8}u_2 - \frac{1}{8}u_1 - \frac{3}{8}u_0.
\end{aligned}
\tag{1}
$$

5

This equation uses the notation of Eq. (13) from the original manuscript[1], where $u_k$ is the value of $k$-th singularity, and $u_0 = 2u_1 - u_2$. Additionally, the plasmonic root in the context of eigenpermittivity modes tends to wander further into the negative half of the complex plane. As such, we place an additional contour underneath this enlarged contour to capture any wayward plasmonic roots. For our purposes, we choose a contour defined by

$$c_p = c_1 - ir_1,$$
$$r_p = r_1.$$
(2)

This additional contour can be further enlarged to cover more of the search space. This does not risk numerical difficulties, since the contour is not expected to enclose many roots, if at all, and is situated in a relatively featureless region of the of search space. An example of this contour is displayed in Figure 2(a). If necessary, the contour can be further enlarged to cover even areas with known roots and singularities by running the additional contour last, and deflating the additional contour of all known roots and singularities. This ensures that the additional contour will not contain more than 5 new roots, which is necessary for the stability of the Newton identities.

For higher-order roots, especially at long wavelength, we employ elliptical contours as roots may wander much farther along the imaginary axis in comparison to the distance between consecutive singularities on the real axis, as shown in Figure 2(b). To make the root search more robust, we also implement an adaptive scheme to search further deep into the imaginary axis of the complex plane until a root is found, i.e.,

$$c_k = c_k \pm l * r_k,$$
$$r_k = r_k.$$
(3)

Here, $l$ is a integer and its value is incremented until a root is found for every contour.

The second revision to the method involves a rescaling of the search variable. In the original implementation, either $\epsilon_c$ or $\beta$ was designated to be the search variable. These parameters are related by the dispersion relation for homogeneous space,

$$\alpha_c^2 + \beta^2 = k^2 \epsilon_c \mu_c,$$
(4)

where $\alpha_c$ is the in-plane propagation constant, $\beta$ is the propagation constant along the cylinder, $k = \omega/c$ is the free space wavenumber, and $\epsilon_c$ and $\mu_c$ are the permittivity and permeability of the cylinder. However, these search

variables encountered numerical problems, for example at long wavelengths, where the roots scale as $1/k^2$. We revise the method to use either $(\alpha_c a)^2$ or $(\beta a)^2$ as the search variable. This ensures that the attraction basins exhibit greater invariance with respect to changes in $a$. In addition, we search for $(\alpha_c a)^2$ rather than $\alpha_c a$, for example, since the latter would result in a duplication of the complex search space. For the implementation of argument principle method, we provide the explicit expressions of the derivatives of fiber dispersion relation for the updated search variables in Appendix A. Additionally, we also provide the expressions of the field profiles of $\beta$ and $\epsilon$ fiber modes and their normalization constants in Appendix B.

## 3. Implementation of the algorithm to other geometries

### 3.1. Slab Waveguide

We now turn to extending the algorithm to a planar step-index slab waveguide which consists of three layers, a guiding layer, surrounded by a cover and a substrate as shown in Fig. 3. We denote the permittivities and permeabilities of these layers as $\epsilon_f$ and $\mu_f$, $\epsilon_c$ and $\mu_c$, and $\epsilon_s$ and $\mu_s$, respectively. The guiding layer is infinite in the $y$-$z$ plane and finite along the $x$-axis, with thickness $a$.
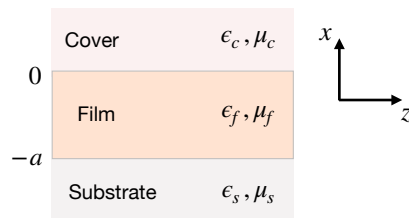


FIGURE 3: *Schematic of slab waveguide geometry shown in $x - z$ plane, with $y$-axis pointing out of the paper.*

In slab waveguides, both transverse electric (TE) and transverse magnetic (TM) modes are supported. We treat these in turn. First, the dispersion relation of TE modes is [2]

$$\frac{\alpha_f^2 - \gamma_c \gamma_s}{\alpha_f} \tan(\alpha_f a) - \gamma_c - \gamma_s = 0. \tag{5}$$

Here, the parameter $\alpha_f$ is the propagation constant along the $x$-direction in the guiding layer, while $\gamma_c$ and $\gamma_s$ are attenuation constants along the

$x$-direction in the cover and substrate layers,

$$\alpha_f^2 = k^2\epsilon_f\mu_f - \beta^2, \qquad \gamma_c^2 = \beta^2 - k^2\epsilon_c\mu_c, \qquad \gamma_s^2 = \beta^2 - k^2\epsilon_s\mu_s \qquad (6)$$

where $k$ is the wavenumber in free-space and $\beta$ is the in-plane propagation constant along $z$-direction. In this dispersion relation, we can set either $(\beta a)^2$, or $\epsilon_f$ as the eigenvalue or search variable.

Similarly, the dispersion relation for TM modes is

$$\frac{\alpha_f^2\epsilon_c\epsilon_s - \epsilon_f^2\gamma_c\gamma_s}{\alpha_f\epsilon_f} \tan(\alpha_f a) - \epsilon_c\gamma_s - \epsilon_s\gamma_c = 0. \qquad (7)$$

The forms (5) and (7) are traditionally used to describe bound (i.e., below the light line) waveguide ($\beta$) modes, yet, they are also suitable to describe radiative modes (i.e., above the light line). In this case, it is important to note that the radiative nature (i.e., $\gamma_{c/s}$ being complex) is accompanied by leakage (i.e., a non-zero imaginary part of $\beta$), which reflects the non-Hermitian nature of the problem. This description contrasts the potentially more standard Hermitian description of the radiative modes as a continuum [29, 30] for which there is no leakage (real $\beta$ eigenvalues); this description involves a slightly more complicated spatial field profile (compared to Eqs. (C.1) and (C.5) in Appendix C), i.e., a profile that includes also incoming waves in the cover/substrate. However, this continuous description requires, naturally, a more complicated mathematical treatment.

For $\beta$ modes, the presence of branch-cuts in dispersion relation greatly effects the choice of sign ($\pm$) before the square root functions of cover and substrate attenuation constants. The choice of the Riemann sheet for guided and radiative modes is decided based upon following conditions.Specifically, the attenuation constants of bound modes should have

$$Re(\gamma_{c,s}) > 0, \quad Im(\gamma_{c,s}) > 0, \qquad (8)$$

so that they decay in the cover/substrate, whereas for radiative modes,

$$Re(\gamma_{c,s}) < 0, \quad Im(\gamma_{c,s}) < 0, \qquad (9)$$

such that the mode grows exponentially in the cover/substrate. The conditions (8) and (9) can be attained by repositioning the branch-cut to be along positive imaginary axis.

We obtain the derivatives to dispersion relations (5) and (7) in Appendix D, which are needed for the argument principle method. Next, we

8

demonstrate the numerical example of our algorithm for the slab waveguide for both cases of eigenvalue: $(\beta a)^2$ and $\epsilon_f$.

We demonstrate the numerical example of the algorithm for $(\beta a)^2$ as an eigenvalue for a *symmetrical* slab waveguide with guiding layer permittivity of $\epsilon_f = 12 + i$, and vacuum cover and substrate layers. We show dispersion characteristics ($\beta$ vs $k = \omega/c$) of TE and TM modes of this slab waveguide in Fig. 4, with $\text{Re}(\beta)$ along the horizontal axis and $\text{Im}(\beta)$ in color. The light lines of the substrate (and cover), $k = \beta$, and the guiding layer, $\beta = \sqrt{Re(\epsilon_f)}k$, are shown as grey lines in the plots. In general, mode profile become bound or radiative based on the condition whether $Re(\beta^2)$ is greater than or less than $k^2$ (see Eq. (6)). Due to complex values of $\beta^2$, we cannot obtain a distinctive condition for the bound and radiative modes purely in terms of $Re(\beta)$. Thus, in the dispersion plot 4 we only show guided modes which satisfies $Re(\beta) > k$ and radiative modes with $Re(\beta) < k$.
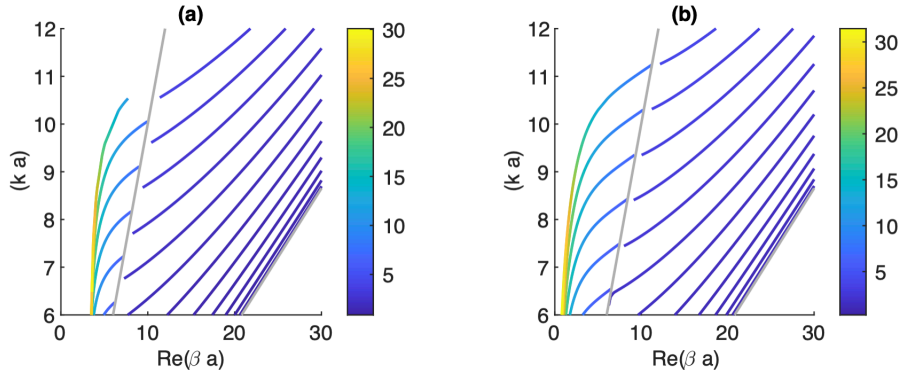


FIGURE 4: *Dispersion relations of modes of the symmetric slab waveguide, produced by our algorithm with complex $(\beta a)^2$ as the search variable, with $Im(\beta)$ represented by color. Plot (a) is of TE modes and plot (b) shows TM modes for a guiding layer of $\epsilon_f = 12 + i$ and vacuum background. The guiding layer thickness a is normalized to 1. The gray line on the left of each figure indicates the light line of vacuum, while the other gray line corresponds to $\beta = \sqrt{12}k$. The modes between the two light lines are guided modes, i.e., their fields are evanescent in the background (i.e., in the cover and substrate layers). The modes above the first light line are radiative modes, their fields grow exponentially in the background.*

Next, we consider $(\alpha_f a)^2$ search variable case. Here, the propagation constant $\beta$ is the independent variable and $\epsilon_f$ of the slab is the dependent variable; the field profiles are defined in Appendix C. We show the dispersion characteristics for this case in Fig. 5. Here, the light lines are vertical since

the wavenumber $k$ is fixed. The bound modes exist to the right of the light line and always have real $\epsilon_f$, while the radiative modes exists to the left of the light line and have complex $\epsilon_f$.
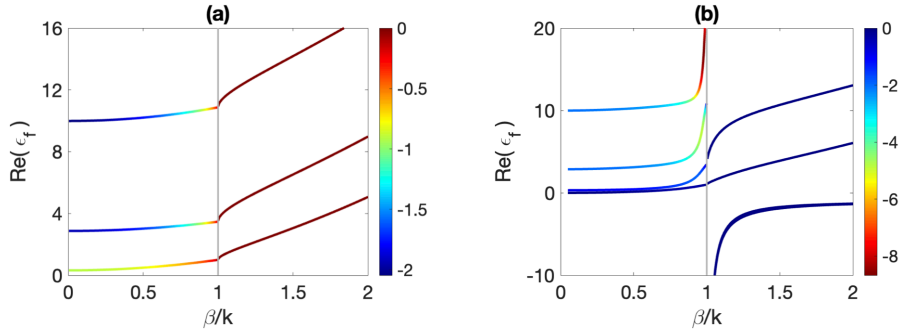


FIGURE 5: *Dispersion relations of eigenpermittivity modes of symmetrical slab waveguide determined using $(\alpha_f a)^2$ search variable. The results are shown in terms of $\epsilon_f$ of slab, with $Im(\epsilon_f)$ indicated by color. Plot (a) is of TE modes and plot (b) shows TM modes for a wave-number $k = 2$, slab thickness $a$ is normalized to 1, and vacuum background. The vertical gray line indicates the light line of vacuum, and the bound modes with only real $\epsilon_f$ exists to the right of the light line, while radiative modes with complex $\epsilon_f$ exists to the left of the light line.*

### 3.2. Spherical scatterers

We treat the secular equation for the modes of a sphere. The relevant parameters are the radius $a$, free-space wavenumber $k$, background permittivity $\epsilon_b$, and sphere permittivity $\epsilon_s$. There are two types of modes: TE, where the component of the electric field along the radial direction is zero, and TM, where the radial magnetic field is zero. Each of these modes are generated by separate equations. For TE, we have [6]

$$\frac{\alpha_s a j'_m(\alpha_s a)}{j_m(\alpha_s a)} = \frac{\alpha_b a h'_m(\alpha_b a)}{h_m(\alpha_b a)}, \tag{10}$$

where $j_m(z)$ and $h_m(z) \equiv h_m^{(1)}(z)$ are the spherical Bessel and Hankel functions of the first kind of order $m$, and the prime denotes differentiation with respect to the entire argument. Propagation constants $\alpha$ are related to material parameters by

$$\alpha = \sqrt{\epsilon}k, \tag{11}$$

10

attaching subscripts $s$ and $b$ to $\alpha$ and $\epsilon$ as appropriate. Equivalently, the secular equation for the TM modes are given by

$$\frac{1}{(\alpha_s a)^2}\left(1 + \frac{\alpha_s a j'_m(\alpha_s a)}{j_m(\alpha_s a)}\right) = \frac{1}{(\alpha_b a)^2}\left(1 + \frac{\alpha_b a h'_m(\alpha_b a)}{h_m(\alpha_b a)}\right). \qquad (12)$$

Once again, to apply the argument principle method, we require the derivatives of (10) and (12). Because of their similarity to the fiber dispersion relation (A.1) and because derivatives spherical and cylindrical Bessel functions obey the same identities, we omit the detailed derivations, and refer the reader to the derivations of Appendix A. As for the geometries studied above the algorithm can be applied for either frequency or permittivity modes.

## 4. Outlook

We have described various improvements and extensions of our argument principle root-search applied to various generic optical structures. We specifically demonstrated propagation constant ($\beta$) and permittivity modes, but our algorithm can also be applied to frequency modes [31] (aka resonant states [32]). In addition to the usefulness of the algorithms detailed above per se, they also provide a convenient starting point for perturbation techniques (in the context of resonant state expansions [32] or re-expansion [16–18]). They can also be extended to simple geometries with more sophisticated physics, such as for systems with anisotropic, nonlocal or non-reciprocal response. Finally, our algorithm can also be applied for the computation of electron wavefunctions in arbitrary potential in atomic calculations [28]. All these potential directions would be explored in future research.

## 5. Acknowledgements.

## Appendix A. Derivatives of the Fiber Dispersion Relation

We update the derivatives used by the argument principle and Newton's methods. We evaluate these explicitly for both $(\alpha_c a)^2$ and $(\beta a)^2$ search

11

variables. We consider the transcendental equation for the step-index fiber dispersion relation,

$$
\left( \frac{\mu_c}{\alpha_c a} \frac{J'_m(\alpha_c a)}{J_m(\alpha_c a)} - \frac{\mu_b}{\alpha_b a} \frac{H'_m(\alpha_b a)}{H_m(\alpha_b a)} \right) \left( \frac{\epsilon_c}{\alpha_c a} \frac{J'_m(\alpha_c a)}{J_m(\alpha_c a)} - \frac{\epsilon_b}{\alpha_b a} \frac{H'_m(\alpha_b a)}{H_m(\alpha_b a)} \right)
$$
$$
- \left( \frac{m\beta}{k} \right)^2 \left( \frac{1}{(\alpha_c a)^2} - \frac{1}{(\alpha_b a)^2} \right)^2 = 0,
\tag{A.1}
$$

which we simplify by introducing the symbols

$$
R^J_m = \frac{J'_m(\alpha_c a)}{\alpha_c a J_m(\alpha_c a)}, \qquad\qquad R^H_m = \frac{H'_m(\alpha_b a)}{\alpha_b a H_m(\alpha_b a)}.
\tag{A.2}
$$

Thus, the dispersion relation can be rewritten as

$$
(\mu_c R^J_m - \mu_b R^H_m)(\epsilon_c R^J_m - \epsilon_b R^H_m) - \left( \frac{m\beta}{k} \right)^2 \left( \frac{1}{(\alpha_c a)^2} - \frac{1}{(\alpha_b a)^2} \right)^2 = 0. \tag{A.3}
$$

The bulk of the calculation involves the derivative

$$
\frac{\partial}{\partial(\alpha_c a)^2} R^J_m = -\frac{1}{2(\alpha_c a)^2} \left[ 1 + 2R^J_m - \frac{J_{m+1}(\alpha_c a) J_{m-1}(\alpha_c a)}{J^2_m(\alpha_c a)} \right]
\tag{A.4}
$$

The defining Bessel differential equation was used in the second equality. Since the Hankel function obeys the same identities, the derivative $\partial R^H_m / \partial(\alpha_b a)^2$ is obtained by the substitution $\alpha_c \to \alpha_b$, $R^J_m \to R^H_m$ and $J_m(\alpha_c a) \to H_m(\alpha_b a)$ in (A.4).

We also have

$$
\frac{\partial \epsilon_c}{\partial(\alpha_c a)^2} = \frac{1}{(ka)^2 \mu_c},
\tag{A.5}
$$

since

$$
\alpha_c^2 + \beta^2 = k^2 \mu_c \epsilon_c.
\tag{A.6}
$$

First consider the derivative of (A.3) with respect to $\epsilon_c$. In order to use (A.4), the chain rule is applied to derive

$$
\mu_c \frac{\partial R^J_m}{\partial(\alpha_c a)^2} [\epsilon_c R^J_m - \epsilon_b R^H_m] + [\mu_c R^J_m - \mu_b R^H_m] \left[ \frac{\partial \epsilon_c}{\partial(\alpha_c a)^2} R^J_m + \epsilon_c \frac{\partial R^J_m}{\partial(\alpha_c a)^2} \right]
$$
$$
+ \frac{2m^2 \beta^2}{(\alpha_c a)^4 k^2} \left( \frac{1}{(\alpha_c a)^2} - \frac{1}{(\alpha_b a)^2} \right),
$$
$$
\tag{A.7}
$$

Now consider the derivative with respect to $(\beta a)^2$, giving

$$\left[\mu_b\frac{\partial R_m^H}{\partial(\alpha_b a)^2} - \mu_c\frac{\partial R_m^J}{\partial(\alpha_c a)^2}\right][\epsilon_c R_m^J - \epsilon_b R_m^H] + [\mu_c R_m^J - \mu_b R_m^H]\left[\epsilon_b\frac{\partial R_m^H}{\partial(\alpha_b a)^2} - \epsilon_c\frac{\partial R_m^J}{\partial(\alpha_c a)^2}\right]$$
$$- \left(\frac{m}{ka}\right)^2 \left(\frac{1}{(\alpha_c a)^2} - \frac{1}{(\alpha_b a)^2}\right)^2 \left[1 + 2(\beta a)^2\left(\frac{1}{(\alpha_c a)^2} + \frac{1}{(\alpha_b a)^2}\right)\right],$$
(A.8)

where we have exploited the fact that

$$\frac{\partial(\alpha_{c,b}\, a)^2}{\partial(\beta a)^2} = -1. \tag{A.9}$$

## Appendix B. Fiber mode fields

In this section, we define the explicit expressions of eigenmode fields of step-index fiber in cylindrical coordinate system.

*Appendix B.1. Eigenpermittivity modes*

The eigenpermittivity mode fields have the following form

$$E_{z,n} = A_n e^{im\theta} e^{i\beta_n z}
\begin{cases}
\dfrac{J_m(\alpha_{c,n} r)}{J_m(\alpha_{c,n} a)} & \text{for } r \le a, \\[2ex]
\dfrac{H_m(\alpha_b r)}{H_m(\alpha_b a)} & \text{for } r > a,
\end{cases} \tag{B.1}$$

$$H_{z,n} = A_n H_0 e^{im\theta} e^{i\beta z}
\begin{cases}
\dfrac{J_m(\alpha_{c,n} r)}{J_m(\alpha_{c,n} a)} & \text{for } r \le a, \\[2ex]
\dfrac{H_m(\alpha_b r)}{H_m(\alpha_b a)} & \text{for } r > a,
\end{cases} \tag{B.2}$$

where

$$H_0 = \left(\frac{1}{(\alpha_{c,n} a)^2} - \frac{1}{(\alpha_b a)^2}\right)\frac{m\beta}{k\left[\dfrac{J_m'(\alpha_{c,n} a)}{\alpha_c a J_m(\alpha_{c,n} a)} - \dfrac{H_m'(\alpha_b a)}{\alpha_b a H_m(\alpha_b a)}\right]}. \tag{B.3}$$

Here, the index $n$ represents the $n^{th}$ eigenpermittivity mode, and the amplitude $A_n$ is the normalization constant of the $n^{th}$ mode, given by

$$A_n = \frac{J_m(\alpha_c a)}{\sqrt{\int_0^a \left[(c1 + c2)\, J_{m-1}(\alpha_c r) dr + (c1 - c2)\, J_{m-1}(\alpha_c r) + J_m(\alpha_c r)\right] dr}}, \tag{B.4}$$

13

where

$$c1 = \frac{\beta^2 - k^2\mu^2 H_0^2}{2\alpha_c^2}, \quad c2 = \frac{i\beta k\mu H_0}{2\alpha_c^2}. \tag{B.5}$$

*Appendix B.2. $\beta$ mode field*

The $\beta$ mode fields have the following form

$$E_{z,n} = A_n e^{im\theta} e^{i\beta_n z} \begin{cases} \dfrac{J_m(\alpha_{c,n}r)}{J_m(\alpha_{c,n}a)} & \text{for } r \leq a, \\[3mm] \dfrac{H_m(\alpha_{b,n}r)}{H_m(\alpha_{b,n}a)} & \text{for } r > a, \end{cases} \tag{B.6}$$

$$H_{z,n} = A_n H_0 e^{im\theta} e^{i\beta_n z} \begin{cases} \dfrac{J_m(\alpha_{c,n}r)}{J_m(\alpha_{c,n}a)} & \text{for } r \leq a, \\[3mm] \dfrac{H_m(\alpha_{b,n}r)}{H_m(\alpha_{b,n}a)} & \text{for } r > a, \end{cases} \tag{B.7}$$

where

$$H_0 = \left( \frac{1}{(\alpha_{c,n}a)^2} - \frac{1}{(\alpha_{b,n}a)^2} \right) \frac{m\beta_n}{k \left[ \dfrac{J'_m(\alpha_{c,n}a)}{\alpha_c a J_m(\alpha_{c,n}a)} - \dfrac{H'_m(\alpha_{b,n}a)}{\alpha_{b,n}a H_m(\alpha_{b,n}a)} \right]}. \tag{B.8}$$

Here, the index $n$ represents the $n^{th}$ eigenvalue of $\beta$, and the amplitude $A_n$ is the normalization constant of the $n^{th}$ mode computed as in [33].

## Appendix C. Slab waveguide Modal fields

*Appendix C.1. $\beta$ mode fields:*

In this subsection, we define the explicit expressions of $\beta$ mode fields of the slab waveguide and its normalization factor. For TE modes, the electric field is transverse to the plane of incidence ($x$-$z$ plane); thus, its mode profile is expressed by the y-component of the electric field, i.e.,

$$E_{y,n}(x,z) = A_n^{TE} e_n(x) e^{i\beta_n z}, \tag{C.1}$$

where

$$e_n(x) = \begin{cases} \cos(\phi_n^{TE}) e^{-\gamma_c x}, & \text{for } x \geq 0, \\ \cos\left(\alpha_{f,n}x + \phi_n^{TE}\right), & \text{for } -a \leq x \leq 0, \\ \cos\left(\alpha_{f,n}a - \phi_n^{TE}\right) e^{\gamma_s(x+a)}, & \text{for } x \leq -a, \end{cases} \tag{C.2}$$

14

and

$$\phi_n^{TE} = \tan^{-1}\left[\frac{\gamma_{c,n}}{\alpha_{f,n}}\right].\tag{C.3}$$

Here, the index $n$ represents the $n^{th}$ eigenvalue of $\beta$, and the amplitude $A_n^{TE}$ is the normalization constant of the $n^{th}$ mode, given by

$$A_n^{TE} = \sqrt{\frac{1}{\frac{1}{2\gamma_c}\left[e_n(0)\right]^2 + \frac{1}{2\gamma_S}\left[e_n(-a)\right]^2 + \int_{-a}^{0}\left[e_n(x)\right]^2\,dx}}.\tag{C.4}$$

For TM modes, we define by the y-component of the magnetic field

$$H_{y,n}(x,z) = A_n^{TM}\,h_n(x)\,e^{i\beta_n z},\tag{C.5}$$

where

$$h_n(x) = \begin{cases} \cos(\phi_n^{TM})\,e^{-\gamma_c x}, & \text{for } x \geq 0, \\ \cos\left(\alpha_{f,n}x + \phi_n^{TM}\right), & \text{for } -a \leq x \leq 0, \\ \cos\left(\alpha_{f,n}a - \phi_n^{TM}\right)\,e^{\gamma_s(x+a)}, & \text{for } x \leq -a, \end{cases}\tag{C.6}$$

and

$$\phi_n^{TM} = \tan^{-1}\left[\frac{\epsilon_f\,\gamma_{c,n}}{\epsilon_c\,\alpha_{f,n}}\right].\tag{C.7}$$

The normalization factor $A_n^{TM}$ is given by

$$A_n^{TM} = \sqrt{\frac{2k_0^2}{c_1\left[h_n(0)\right]^2 + c_2\left[h_n(-a)\right]^2 + \frac{2}{\epsilon_f^2}\int_{-a}^{0}\left[\beta_n^2\left[h_n(x)\right]^2 + \left[h_n'(x)\right]^2\right]\,dx}},\tag{C.8}$$

where

$$c_1 = \left(\frac{\beta_n^2 + \gamma_{c,n}^2}{\epsilon_c^2\,\gamma_{c,n}}\right), \qquad c_2 = \left(\frac{\beta_n^2 + \gamma_{s,n}^2}{\epsilon_s^2\,\gamma_{s,n}}\right).\tag{C.9}$$

*Appendix C.2. Eigenpermittivity modes*

Now, we will look into field profile and normalization factor of eigenpermittivity modes. For TE modes, the mode profile is expressed by the y-component of the electric field, i.e.,

$$E_{y,n}(x,z) = A_n^{TE}\,e^{i\beta z}\begin{cases} \cos(\phi_n^{TE})\,e^{-\gamma_c x}, & \text{for } x \geq 0, & \text{(cover)} \\ \cos\left(\alpha_{f,n}x + \phi_n^{TE}\right), & \text{for } -a \leq x \leq 0, & \text{(film)} \\ \cos\left(\alpha_{f,n}a - \phi_n^{TE}\right)\,e^{\gamma_s(x+a)}, & \text{for } x \leq -a, & \text{(substrate)} \end{cases}\tag{C.10}$$

15

where the index $n$ represents the $n^{th}$ eigenpermittivity mode, and the amplitude $A_n^{TE}$ is the normalization constant of the $n^{th}$ mode, given by

$$A_n^{TE} = \sqrt{\frac{2\alpha_{f,n}}{\alpha_{f,n}a + \sin(\alpha_{f,n}a)\cos(\alpha_{f,n}a - 2\phi_n^{TE})}}. \tag{C.11}$$

Here,

$$\phi_n^{TE} = \tan^{-1}\left[\frac{\gamma_c}{\alpha_{f,n}}\right]. \tag{C.12}$$

For TM modes, we define by the y-component of the magnetic field

$$H_{y,n}(x,z) = A_n^{TM}\, e^{i\beta z} \begin{cases} \cos(\phi_n^{TM})\, e^{-\gamma_c x}, & \text{for } x \geq 0, \\ \cos\left(\alpha_{f,n}x + \phi_n^{TM}\right), & \text{for } -a \leq x \leq 0, \\ \cos\left(\alpha_{f,n}a - \phi_n^{TM}\right)\, e^{\gamma_s(x+a)}, & \text{for } x \leq -a, \end{cases} \tag{C.13}$$

where

$$\phi_n^{TM} = \tan^{-1}\left[\frac{\epsilon_{f,n}\,\gamma_c}{\epsilon_c\,\alpha_{f,n}}\right], \tag{C.14}$$

and

$$A_n^{TM} = \sqrt{\frac{2k^2\epsilon_{f,n}^2}{\left[\beta^2 + \alpha_{f,n}^2\right]a + \left(\dfrac{\beta^2 - \alpha_{f,n}^2}{\alpha_{f,n}}\right)\sin\left[\alpha_{f,n}a\right]\cos\left[\alpha_{f,n}a - 2\phi_n^{TM}\right]}}. \tag{C.15}$$

## Appendix D. Derivatives of the Slab Dispersion Relation

In this section, we obtain the derivatives of the slab waveguide dispersion equation required in implementation of the argument principle method for types of search variables: $(\alpha_f a)^2$ and $(\beta a)^2$.

### Appendix D.1. TE modes

For notational simplicity, we introduce a new symbol for the TE dispersion equation (5),

$$R_{\text{TE}} = \frac{(\alpha_f a)^2 - (\gamma_c a)(\gamma_s a)}{\alpha_f a}. \tag{D.1}$$

Thus, (5) can be rewritten as

$$R_{\text{TE}} \tan(\alpha_f a) - \gamma_c a - \gamma_s a = 0. \tag{D.2}$$

16

The bulk of the calculation involves the derivatives of $R_{\text{TE}}$

$$\frac{\partial R_{\text{TE}}}{\partial(\alpha_f a)^2} = \frac{(\alpha_f a)^2 + (\gamma_c a)(\gamma_s a)}{2(\alpha_f a)^3},$$

$$\frac{\partial R_{\text{TE}}}{\partial(\gamma_c a)^2} = -\frac{\gamma_s a}{2(\alpha_f a)\gamma_c a}, \qquad \frac{\partial R_{\text{TE}}}{\partial(\gamma_s a)^2} = -\frac{\gamma_c a}{2(\alpha_f a)\gamma_s a}. \tag{D.3}$$

We also know

$$\frac{\partial \epsilon_f}{\partial(\alpha_f a)^2} = \frac{1}{(ka)^2 \mu_f}, \tag{D.4}$$

since

$$(\alpha_f a)^2 + \beta^2 = k^2 \mu_f \epsilon_f. \tag{D.5}$$

By using the chain rule, we can obtain the derivative of the dispersion equation (D.2) with respect to $(\alpha_f a)^2$ as

$$\left( \frac{\partial R_{\text{TE}}}{\partial(\alpha_f a)^2} \tan(\alpha_f a) + \frac{R_{\text{TE}}}{2\alpha_f a} \sec^2(\alpha_f a) \right) = 0. \tag{D.6}$$

Next, we consider the derivative of (D.2) with respect to $(\beta a)^2$

$$\left( -\frac{\partial R_{\text{TE}}}{\partial(\alpha_f a)^2} + \frac{\partial R_{\text{TE}}}{\partial(\gamma_c a)^2} + \frac{\partial R_{\text{TE}}}{\partial(\gamma_s a)^2} \right) \tan(\alpha_f a) - \frac{R_{\text{TE}}}{2\alpha_f a} \sec^2(\alpha_f a) - \frac{1}{2\gamma_c a} - \frac{1}{2\gamma_s a} = 0, \tag{D.7}$$

where we exploited the fact that

$$\frac{\partial(\alpha_f a)^2}{\partial(\beta a)^2} = -1, \qquad \frac{\partial(\gamma_{c,s} a)^2}{\partial(\beta a)^2} = 1. \tag{D.8}$$

*Appendix D.2. TM modes*

For simplification, we introduce a symbol for the TM dispersion relation (7),

$$R_{\text{TM}} = \frac{(\alpha_f a)^2 \epsilon_c \epsilon_s - \epsilon_f^2 (\gamma_c a)(\gamma_s a)}{(\alpha_f a)\epsilon_f}. \tag{D.9}$$

Thus, (7) can be rewritten as

$$R_{\text{TM}} \tan(\alpha_f a) - \epsilon_c \gamma_s - \epsilon_s \gamma_c = 0. \tag{D.10}$$

The derivatives of $R_{\text{TM}}$ is given by

$$\frac{\partial R_{\text{TM}}}{\partial(\alpha_f a)^2} = \frac{1}{(\alpha_f a)\epsilon_f} \left[ \epsilon_c \epsilon_s - (\gamma_c a)(\gamma_s a) \frac{\partial \epsilon_f^2}{\partial(\alpha_f a)^2} \right] - \frac{R_{\text{TM}}}{2(\alpha_f a)^2} - \frac{R_{\text{TM}}}{\epsilon_f} \frac{\partial \epsilon_f}{\partial(\alpha_f a)^2},$$

$$\frac{\partial R_{\text{TM}}}{\partial(\gamma_c a)^2} = -\frac{\epsilon_f(\gamma_s a)}{2(\alpha_f a)\gamma_c a}, \qquad \frac{\partial R_{\text{TM}}}{\partial(\gamma_s a)^2} = -\frac{\epsilon_f(\gamma_c a)}{2(\alpha_f a)\gamma_s a}. \tag{D.11}$$

We also know that

$$\frac{\partial \epsilon_f}{\partial (\alpha_f a)^2} = \frac{1}{(ka)^2 \mu_f}, \qquad \frac{\partial \epsilon_f^2}{\partial (\alpha_f a)^2} = \frac{2\epsilon_f}{(ka)^2 \mu_f}, \qquad \text{(D.12)}$$

from the definition

$$\alpha_f^2 + \beta^2 = k^2 \mu_f \epsilon_f. \qquad \text{(D.13)}$$

Now we can show that the derivative of the TM dispersion equation (D.10) with respect to $(\alpha_f a)^2$ as

$$\left( \frac{\partial R_{\text{TM}}}{\partial (\alpha_f a)^2} \tan(\alpha_f a) + \frac{R_{\text{TM}}}{2\alpha_f a} \sec^2(\alpha_f a) \right) = 0. \qquad \text{(D.14)}$$

Similarly, the derivative of (D.10) with respect to $(\beta a)^2$ is derived as

$$\left( -\frac{\partial R_{\text{TM}}}{\partial (\alpha_f a)^2} + \frac{\partial R_{\text{TM}}}{\partial (\gamma_c a)^2} + \frac{\partial R_{\text{TM}}}{\partial (\gamma_s a)^2} \right) \tan(\alpha_f a) - \frac{R_{\text{TE}}}{2\alpha_f a} \sec^2(\alpha_f a) - \frac{\epsilon_c}{2\gamma_s a} - \frac{\epsilon_s}{2\gamma_s a} = 0,$$
$$\text{(D.15)}$$

where we used the fact that

$$\frac{\partial (\alpha_f a)^2}{\partial (\beta a)^2} = -1, \qquad \frac{\partial (\gamma_{c,s} a)^2}{\partial (\beta a)^2} = 1. \qquad \text{(D.16)}$$

## References

[1] P. Y. Chen, Y. Sivan, Robust location of optical fiber modes via the argument principle method, Comput. Phys. Commun. 214 (2017) 105–116.

[2] P. Yeh, Optical Waves in Layered Media, 2nd Edition, Wiley-Interscience, 2005.

[3] K. Okamoto, Fundamentals of Optical waveguides, 2nd Edition, Academic Press, 2006.

[4] Q. Bai, M. Perrin, C. Sauvan, J.-P. Hugonin, P. Lalanne, Efficient and intuitive method for the analysis of light scattering by a resonant nano-structure, Opt. Express 21 (2013) 27371.

[5] D. J. Bergman, D. Stroud, in Solid State Physics, H. Ehrenreich and D. Turnbull, eds., Vol. 46, pp. 148-270, Academic Press, 1992.

[6] D. J. Bergman, D. Stroud, Theory of resonances in the electromagnetic scattering by macroscopic bodies, Phys. Rev. B 22 (1980) 3527–3539.

[7] T. Sandu, Eigenmode decomposition of the near-field enhancement in localized surface plasmon resonances of metallic nanoparticles, Plasmonics 8 (2012) 391–402.

[8] N. Liver, A. Nitzan, J. I. Gersten, Local fields in cavity sites of rough dielectric surfaces, Chemical Physics Letters 111 (1984) 449–454.

[9] M. S. Agranovich, B. Z. Katsenelenbaum, A. N. Sivov, N. N. Voitovich, Generalized method of eigenoscillations in diffraction theory, Wiley-VCH, 1999.

[10] K. Li, M. I. Stockman, D. J. Bergman, Enhanced second harmonic generation in a self-similar chain of metal nanospheres, Phys. Rev. B 72 (2005) 153401.

[11] L. Ge, Y. D. Chong, A. D. Stone, Steady-state ab initio laser theory: generalizations and analytic results, Phys. Rev. A 82 (2010) 063824.

[12] O. Schnitzer, Singular perturbations approach to localized surface-plasmon resonance: Nearly touching metal nanospheres, Phys. Rev. B 92 (2015) 235428.

[13] O. Schnitzer, V. Giannini, S. A. Maier, R. V. Craster, Surface plasmon resonances of arbitrarily shaped nanometallic structures in the small-screening length limit, Proc. R. Soc. A 472 (2016) 20160258.

[14] A. Farhi, D. Bergman, Electromagnetic eigenstates and the field of an oscillating point electric dipole in a flat-slab composite structure, Phys. Rev. A 93 (2016) 063844.

[15] P. Y. Chen, D. J. Bergman, Y. Sivan, Generalizing normal mode expansion of electromagnetic green's tensor to open systems, Phys. Rev. Appl. 11 (2019) 044018.

[16] P. Y. Chen, Y. Sivan, E. A. Muljarov, An efficient solver for the generalized normal modes of non-uniform open optical resonators, J. Comp. Phys. 422 (2020) 109754.

[17] N. Kossowski, P. Y. Chen, Q. J. Wang, P. Genevet, Y. Sivan, Scattering by lossy anisotropic scatterers: A modal approach, J. App. Phys. 129 (11) (2021) 113104.

[18] P. Y. Chen, Y. Sivan, Resolving the gibbs phenomenon via a discontinuous basis in a mode solver for open optical systems, J. Comp. Phys. 429 (2021) 110004.

[19] G. Rosolen, P. Y. Chen, B. Maes, Y. Sivan, Overcoming the bottleneck for quantum computations of complex nanophotonic structures: Purcell and förster resonant energy transfer calculations using a rigorous mode-hybridization method, Phys. Rev. B 101 (2020) 155401.

[20] G. Rosolen, B. Maes, Strong multipolar transition enhancement with graphene nanoislands, APL Photonics 6 (2021) 086103.

[21] C. Forestiere, G. Miano, Material-independent modes for electromagnetic scattering, Phys. Rev. B 94 (2016) 201406.

[22] M. Pascale, G. Miano, C. Forestiere, Spectral theory of electromagnetic scattering by a coated sphere, J. Opt. Soc. Am. B 34 (7) (2017) 1524–1535.

[23] C. Forestiere, G. Miano, G. Rubinacci, A. Tamburrino, R. Tricarico, S. Ventre, Volume integral formulation for the calculation of material independent modes of dielectric scatterers, IEEE Trans. on Ant. and Propagation 66 (2018) 2505.

[24] M. Pascale, G. Miano, R. Tricarico, C. Forestiere, Full-wave electromagnetic modes and hybridization in nanoparticle dimers, Sci. Rep. 9 (2019).

[25] S. Rao, P. Y. Chen, G. LeSaux, Y. Sivan, Generalised normal mode expansion method for open and lossy periodic structures, J. Opt. Soc. Am. B 39 (2022) 1338–1347.

[26] P. Y. Chen, Y. Greenberg, Y. Sivan, Wide frequency band expansion of permittivity normal modes, J. Opt. Soc. Am. B 39 (2022) 2387–2394.

[27] G. Y. Slepyan, D. Mogilevtsev, I. Levie, A. Boag, Modeling of multimodal scattering by conducting bodies in quantum optics: The method of characteristic modes, Phys. Rev. Appl. 18 (2022) 014024.

[28] N. Moiseyev, Non-hermitian Quantum Mechanics, Cambridge University Press, 2011.

[29] W. Chew, Waves and Fields in Inhomogeneous media, Wiley-IEEE Press, 1999.

[30] D. Marcuse, Theory of dielectric optical waveguides, Academic, 1972.

[31] P. Lalanne, W. Yan, K. Vynck, C. Sauvan, J.-P. Hugonin, Light interaction with photonic and plasmonic resonances, Lasers and Photonics Review 12 (2017) 1700113.

[32] E. A. Muljarov, W. Langbein, R. Zimmermann, Brillouin-wigner perturbation theory in open electromagnetic systems, Europhys. Lett. 92 (2010) 50010.

[33] S. Upendar, I. Allayarov, M. A. Schmidt, T. Weiss, Analytical mode normalization and resonant state expansion for optical fibers - an efficient tool to model transverse disorder, Opt. Exp. 26 (2018) 22536.